

# THE EFFECT OF A SYNTHETIC JET ON THE PRESSURE DISTRIBUTION OF A FLAT PLATE

Young-Hwan KIM\*, K.P.Garry\*\*

\*Emirates Aviation University, UAE \*\*Cranfield University, UK

**Keywords:** *Synthetic Jet, Piezoelectric, Boundary layer, Vortex, Flow Control*

## Abstract

The effect of a rectangular synthetic jet on the surface static pressure distribution on a flat plate in a zero freestream pressure gradient at Reynolds numbers in the range  $8 \times 10^5 < Re_c < 1.8 \times 10^6$ , is investigated with a view to potential boundary layer flow control. The increment in surface static pressure distribution, relative to that of the undisturbed flat plate, is compared with that of conventional vane type vortex generator. Changes in pressure consistent with the formation of a longitudinal vortex are seen to be dependent on Reynolds number and slot yaw angle. The lateral influence of the synthetic jet efflux at axial stations ( $x, mm$ ) between  $-200 < x < 300$  is used to quantify the potential impact of the synthetic jet flowfield compared to that of a conventional vortex generator. Regions of +ve and -ve pressure changes are seen to be dependent on Reynolds number.

## 1 Design of Piezoelectric-driven Synthetic Jet Generator

A piezoelectric diaphragm is a thin metal plate with a piezoelectric ceramic adhered to one face. A high frequency alternating voltage will cause the diaphragm to vibrate as a result of the difference of deformation ratio between the two materials. A piezoelectric diaphragm supplied by Murata Manufacturing Company (Product reference: 7BB-50M-1) is used to fabricate the Synthetic Jet Generator (SJG) used in this study. This particular diaphragm is designed for use in acoustic devices; it consists of a 50mm diameter nickel-plated brass disc with a 25mm diameter piezoelectric ceramic film on one face.[1]

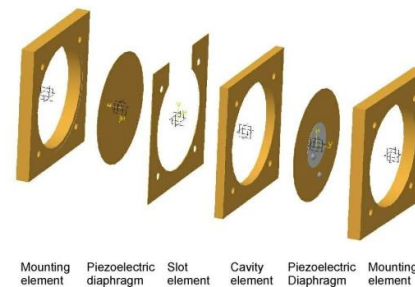


Fig. 1. Expanded view of key SJG components

## 2 Experimental Arrangement

The SJG used in this study is mounted beneath the surface of a flat plate, within a flush-fitting turntable, which can be rotated through 360 degrees to facilitate a change of SJG slot yaw angle ( $\beta$ ) relative the free stream, see Figure 2. Slot yaw angle is known to be a significant factor in determining the strength of the longitudinal vortex that forms downstream of the slot as a result of the SJG efflux, see Kim [11]

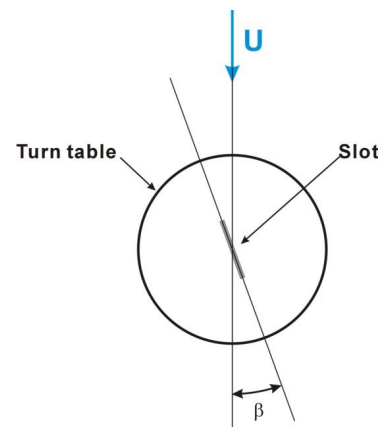


Fig. 2. Plan elevation of turntable within the flat plate and definition of slot yaw angle ( $\beta$ )

Figure 3 depicts the flat plate coordinate system, the origin of which is the centre of the SJG slot, located 25cm downstream of the flat plate leading edge. To aid data analysis, locations on the flat plate are non-dimensionalised using the slot width ( $H=0.5\text{mm}$ ). Individual surface static pressure tapings are connected to a 48-port Scanivalve coupled to a Setra 239 differential pressure transducer pressure scanning system by means of flexible pneumatic tubes, shown in Figure 4. As these could not be located within the SJG assembly, the static pressure distribution in the region adjacent to the slot ( $-4\text{cm} < x < 3\text{cm}$ ) cannot be measured - this area is referred to as a "blind area" in this study, see Figure 5.

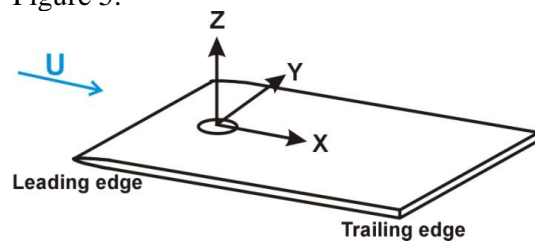


Fig. 3. Flat plate coordinate system with SJG

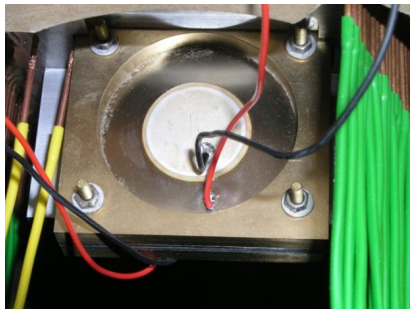


Fig 4. SJG assembly mounted beneath the the flat plate

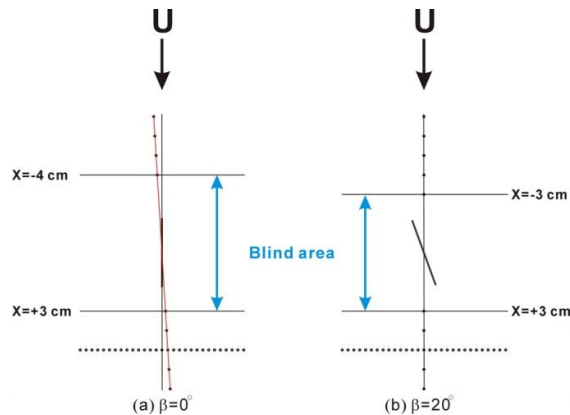


Fig 5. Schematic layout of SJG slot and adjacent rows of pressure tapings in the flat plate to illustrate the 'blind area'

The surface static pressure distribution on the plate is measured using an array of six spanwise rows of 29 pressure tapings (3mm lateral spacing, centre to centre covering the lateral range  $-42\text{mm} < Y < +42\text{mm}$ ). The pressure tapping rows cover axial locations in the range from  $X=50\text{mm}$  to  $X=300\text{mm}$  in 50mm increments. In addition, this matrix is supplemented by a streamwise row of 46 pressure tapings along the plate lateral centreline at 10mm increments. This row extends from  $x = -200\text{mm}$  (upstream of the SJG) to  $x = 300\text{mm}$  (downstream of the SJG). This arrangement is depicted schematically in Figure 6. Individual pressure tapings are fabricated from brass tube, which has 1.5mm external diameter and 0.9mm internal diameter. Each pressure port is sampled at a frequency ( $F_s$ ) of 3 KHz for a sampling period ( $T_s$ ) of 3 seconds. A 3 second settling period is allowed before each measurement.

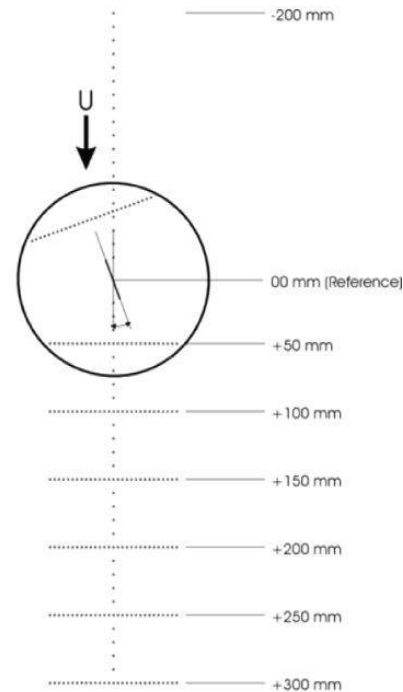


Fig. 6. Static pressure tapping arrangement

## 2.1 Vortex Generator

A conventional vane type vortex generator (VG) was mounted on the plate at the same location as the SJG to facilitate pressure data for

comparison purposes. The VG has a cropped delta planform with a chord ( $L$ ) of 35mm – the same as that of the SJG slot length. The VG height is 5mm, equivalent to 152% of the maximum local boundary layer thickness (which was measured for the conditions  $U=8.53\text{m/s}$ ,  $Re_x=8.17\times 10^5$ ). The VG was installed over the SJG slot with an inclination ( $\beta$ ) of 20 degrees to the free stream, the same as the optimum slot yaw angle for vortex generation. Figure 7 illustrates the design and installation of VG.

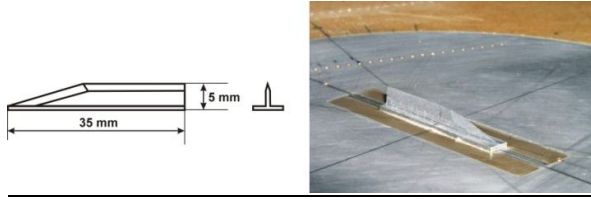


Fig. 7. Conventional vane type vortex generator

### 3 Discussion of Results

The SJG is excited at a fixed acoustic resonance frequency (F1) of 1.5 KHz, which results in a mean jet velocity of 11.05 m/s. Because the mean synthetic jet velocity is constant, the jet momentum coefficient ( $C_{\mu}$ ) can be varied only by the changing the freestream velocity ( $U$ )

Synthetic Jet velocities @ resonance frequency			
Max	Min	RMS	Mean
56.10 m/s	2.15 m/s	18.14 m/s	11.05 m/s

The pressure coefficient ( $C_p$ ) and pressure coefficient difference ( $\Delta C_p$ ) are defined as the followings. The freestream data measured using a Pitot-static tube above the flat plate.

$$C_p = (p - p_{\infty}) / q_{\infty} \quad (1)$$

$$\Delta C_p = C_{p_{on}} - C_{p_{off}} \quad (2)$$

Where,

$p$ : Local static pressure

$p_{\infty}$ : Freestream static pressure

$q_{\infty}$ : Freestream dynamic pressure

$\rho_{\infty}$ : Freestream density

$U$ : Freestream velocity

$C_{p_{on}}$ :  $C_p$  with SJG-On or with VG

$C_{p_{off}}$ :  $C_p$  with SJG-Off or without VG

### 3.1 Spanwise static pressure distribution around the vortex core

An example of the spanwise pressure increment distribution in a plane at  $x = 50\text{mm}$  as a result of the SJG is shown in Figure 8. This condition corresponds to a free stream velocity of  $U=8.53\text{m/s}$  and the variation of pressure coefficient increment (SJG on – SJG off)  $\Delta C_p$ , is similar to that seen as a result of using a conventional VG in a study by Mahalingam et al.[2]. Note that VR corresponds to the jet “Velocity Ratio” between mean synthetic jet velocity and freestream velocity. The core of the vortex created by the vane type VG, is located near the suction peak. The location of the core is approximated by the two vertical broken lines in Figure 8. The direction of rotation is considered to be counter-clockwise when viewed from downstream. The spanwise distribution  $\Delta C_p$  produced by a synthetic jet is similar to that of the vane type vortex generator. The suction peak appears at nominally  $Y/H=6$  and the pressure distribution suggests a counter-clockwise rotation. At this condition ( $Re_x=1.75\times 10^5$ ), the SJG produces a greater suction and pressure increment peak than that of the vane type vortex generator.

According to the study of Zhang et al.[3], the streamwise vortex creates regions of local upwash and downwash within the boundary layer, the later responsible for momentum transfer which results in a “*thining effect*” on the boundary layer that enhances its ability to resist flow separation. Given that both the SJG ( $\beta=20^\circ$ ) and the vane type VG ( $\beta=20^\circ$ ) exhibit surface static pressure increments consistent with the formation of counter-clockwise rotating vortex structure, the SJG can be considered as a potential alternative to a conventional VG for flow control.

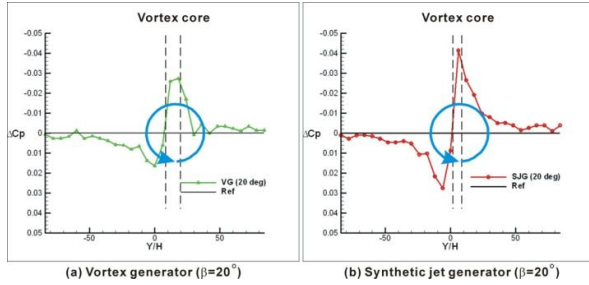


**Fig. 8.** Vortex structure interpretation by  $\Delta C_p$  distribution  
 ( $C_\mu=5.99 \times 10^{-4}$ ,  $VR=1.30$ ,  $X=50\text{mm}$ ,  $Re_x=1.75 \times 10^5$ )

Figure 9 is a schematic of a possible synthetic jet slot arrangement on practical aerodynamic surfaces. An SJG array with same slot orientation will result in a row of vortices with the same rotation sign. However, an arrangement of synthetic jet slots with alternating slot yaw angles will result in vortices with different rotation directions. This concept is routinely used for practical flow control applications.

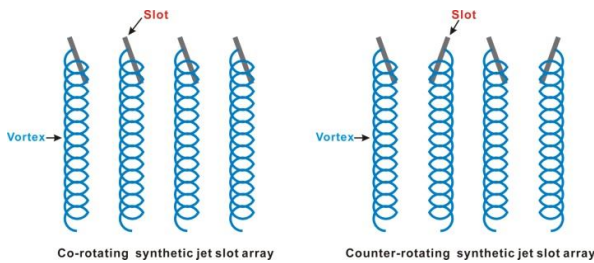


**Fig. 9.** Proposed arrangement of synthetic jet slot arrangement for practical application

### 3.2 Data repeatability

The repeatability of the pressure increment distribution data ( $\Delta C_p$ ) is investigated in view of the fact that the corresponding pressures at the Reynolds numbers ( $Re_x$ ) considered are very low and measurement uncertainty may be important. The degree of uncertainty is expressed by the error bars in Figure 10. Each data point is based on the mean of three measurements which are taken at the same test conditions. The error bars correspond to the standard deviation ( $\sigma$ ) around the mean  $\Delta C_p$ . Whilst it can be seen that there is greater uncertainty at the lower Reynolds number (high-VR and high- $C_\mu$ ), it is clear that the

measurement repeatability is such as to suggest that the pressure increments measured are the result of a characteristic flow phenomenon.

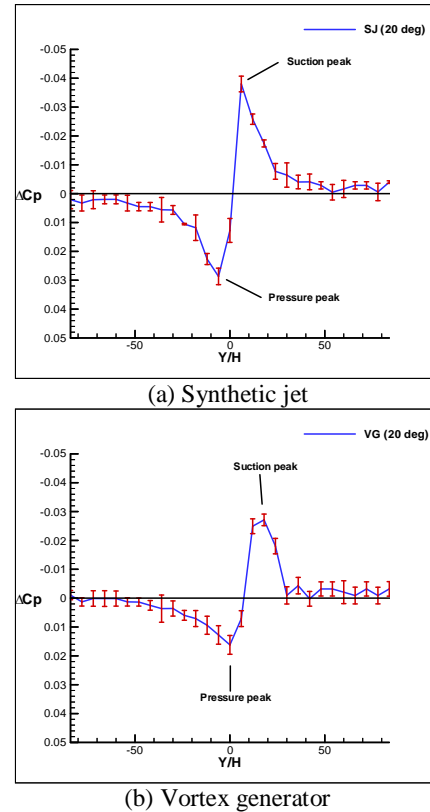


**Fig. 10.** The repeatability of  $\Delta C_p$  due to synthetic jet and vortex generator ( $X=50\text{mm}$ ,  $\beta=20^\circ$ ,  $U=8.53\text{m/s}$ ,  $C_\mu=5.99 \times 10^{-4}$ ,  $VR=1.30$ ,  $Re_x=1.75 \times 10^5$ )

### 3.3 Effect of streamwise distance

The development of the vortical flow structure downstream of both the synthetic jet and vane VG is investigated by considering the lateral pressure distribution at different axial locations within the zero pressure gradient boundary layer on the flat plate.

The lateral displacement of the vortex is detected in each case, Figure 11 shows that the suction region moves in the +ve Y direction with increasing x and reduces in magnitude. This is assumed to relate to the lateral displacement of the vortex core and either its breakdown or increased vertical displacement from the plate surface.

**THE EFFECT OF A SYNTHETIC JET ON THE PRESSURE DISTRIBUTION OF A FLAT PLATE**

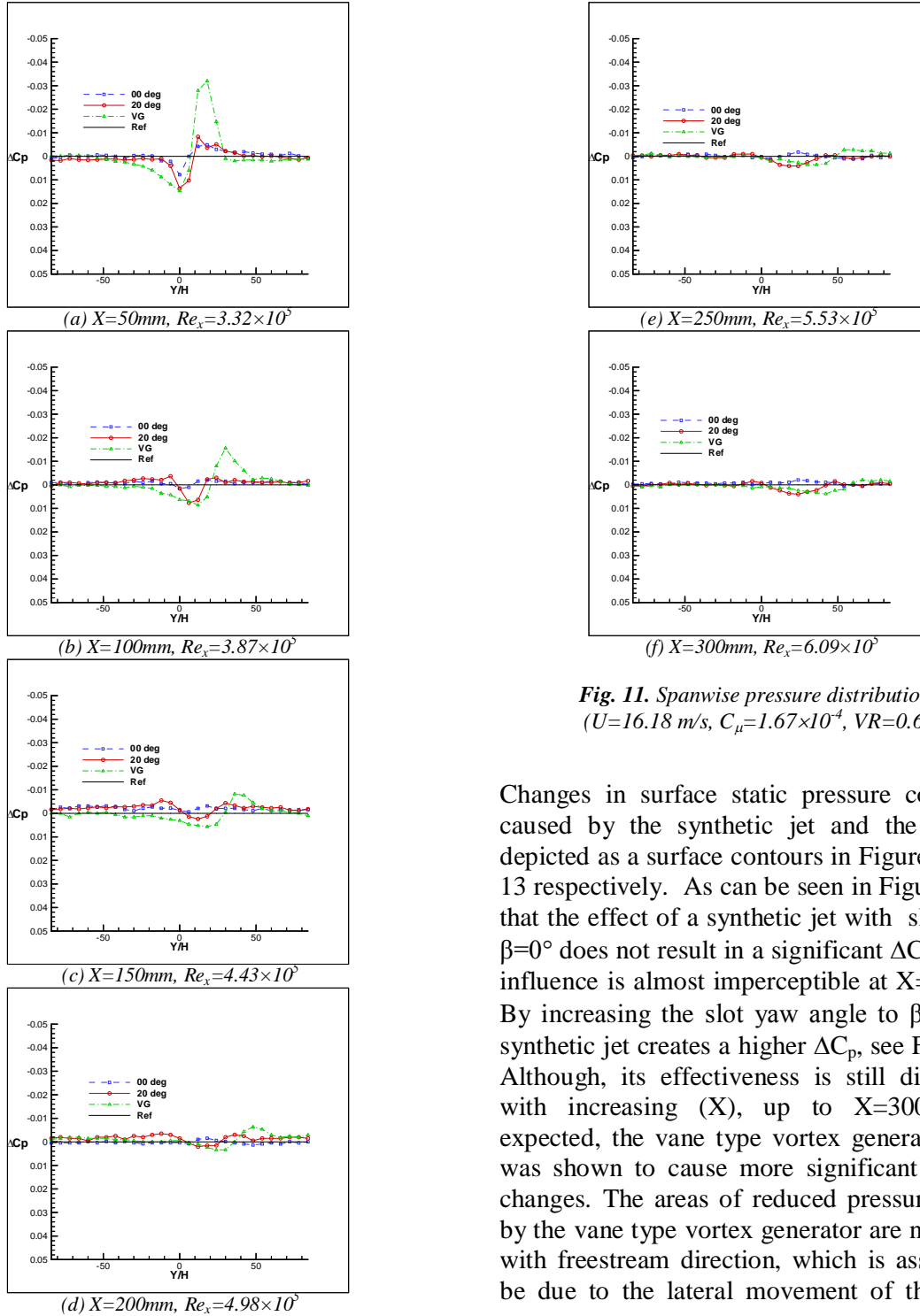
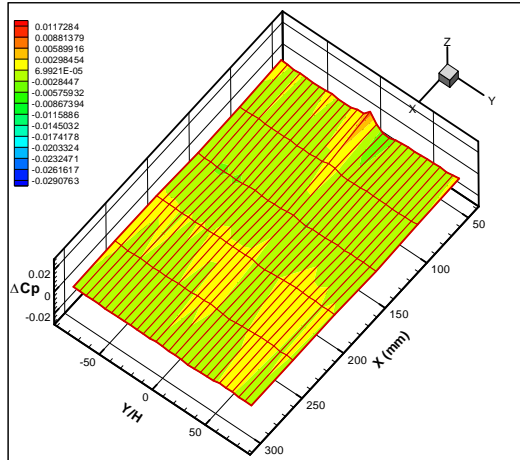
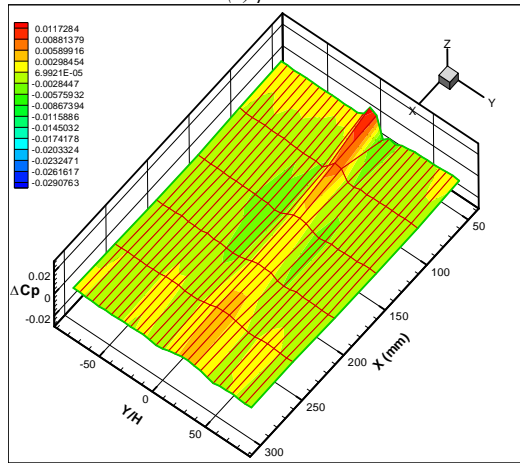


**Fig. 11.** Spanwise pressure distributions ( $U=16.18\text{ m/s}$ ,  $C_{\mu}=1.67 \times 10^{-4}$ ,  $VR=0.68$ )

Changes in surface static pressure coefficient caused by the synthetic jet and the VG are depicted as surface contours in Figures 12 and 13 respectively. As can be seen in Figure 12(a), that the effect of a synthetic jet with slot angle,  $\beta=0^\circ$  does not result in a significant  $\Delta C_p$ , and its influence is almost imperceptible at  $X=100\text{mm}$ . By increasing the slot yaw angle to  $\beta=20^\circ$  the synthetic jet creates a higher  $\Delta C_p$ , see Fig.12(b). Although, its effectiveness is still diminished with increasing ( $X$ ), up to  $X=300\text{mm}$ , as expected, the vane type vortex generator (VG) was shown to cause more significant pressure changes. The areas of reduced pressure caused by the vane type vortex generator are not in line with freestream direction, which is assumed to be due to the lateral movement of the vortex core.



(a)  $\beta=0^\circ$



(b)  $\beta=20^\circ$

Fig. 12. The effect of synthetic jet to downstream flowfield ( $U=16.18$  m/s,  $VR=0.68$ ,  $C_{\mu}=1.67 \times 10^{-4}$ ,  $Re_c=1.55 \times 10^6$ , zero pressure gradient)

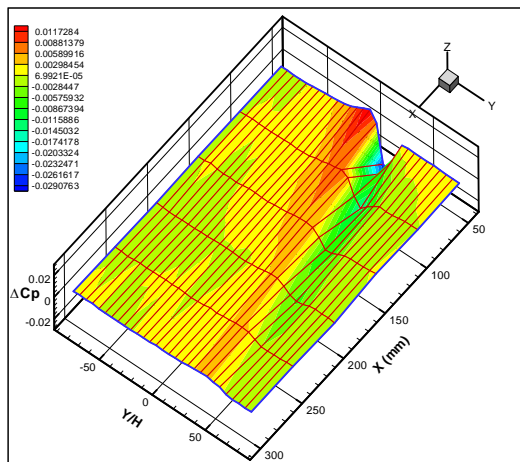
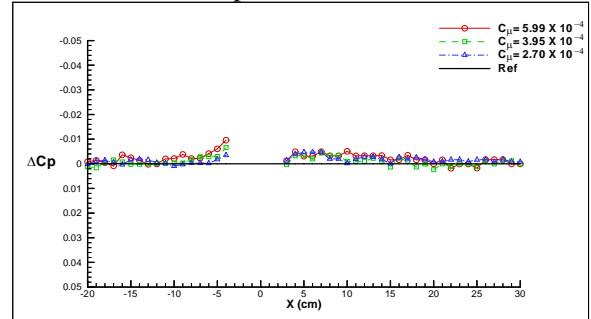


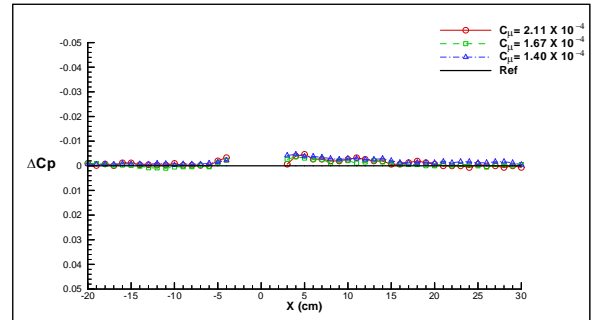
Fig. 13. The effect of vane type vortex generator (VG) to downstream flowfield ( $U=16.18$  m/s,  $Re_c=1.55 \times 10^6$ ,  $\beta=20^\circ$ , zero pressure gradient)

### 3.4 Streamwise pressure change distribution in a zero freestream pressure gradient

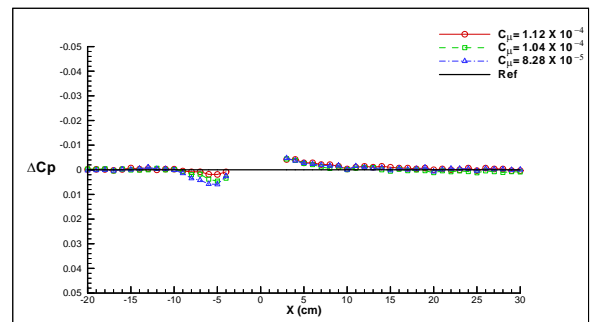
A streamwise  $\Delta C_p$  distribution survey on the zero pressure gradient flat plate was carried out using data from the single row of axial tappings (recognizing the blind area,  $x = -4\text{cm} \sim +3\text{cm}$ ). As can be seen in Figure 14, the synthetic jet affects both the flowfield both downstream and upstream of the slot.



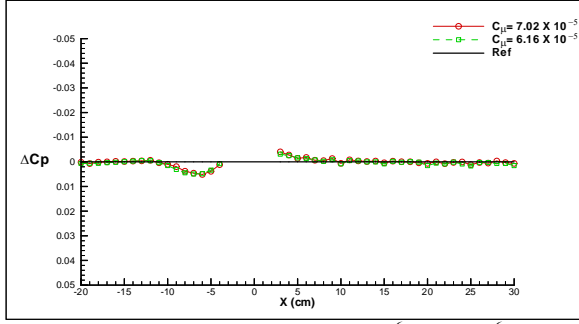
(a)  $VR=1.30-0.87$  ( $Re_c=8.17 \times 10^5 \sim 1.22 \times 10^6$ )



(b)  $VR=0.77-0.63$  ( $Re_c=1.38 \times 10^6 \sim 1.69 \times 10^6$ )



(c)  $VR=0.56-0.48$  ( $Re_c=1.89 \times 10^6 \sim 2.20 \times 10^6$ )



(d)  $VR=0.44\sim 0.42$  ( $Re_c=2.39\times 10^6\sim 2.55\times 10^6$ )

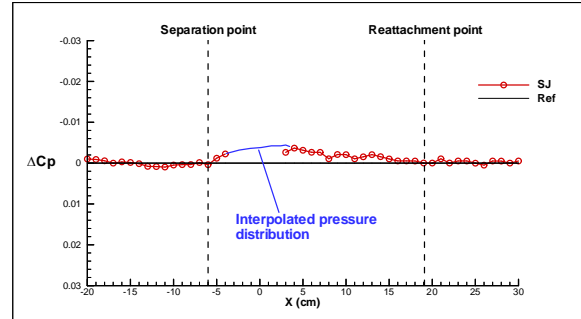
Fig. 14. Streamwise pressure coefficient change by synthetic jet ( $\beta=0^\circ$ )

In view of the low freestream velocity it is difficult to measure static pressure increment distribution at low Reynolds number with great confidence. However, the length of the recirculation region may be affected by synthetic jet velocity ratio (VR), jet momentum coefficient ( $C_\mu$ ), and Reynolds number. A low- $Re_c$  (high- $C_\mu$ ) is expected to cause a long recirculation region and high- $Re_c$  (low- $C_\mu$ ) is expected to result in a short one.

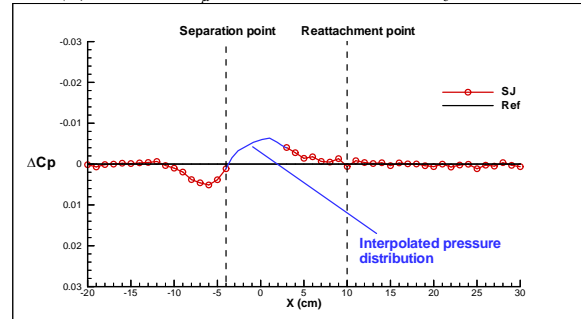
The freestream structure around a circular steady jet nozzle may be considered similar to that of a chimney root. According to the study by Frice et al[4], a horseshoe vortex exists around the steady jet nozzle and a stagnation point exists in front of horseshoe vortex, see Figure 14.

The freestream around a synthetic jet may be similar to that of a steady jet with the formation of a stagnation point in front of the resulting closed re-circulation region (CRR). Figure 15 shows the streamwise  $\Delta C_p$  distribution with the static pressure increment decreasing at low- $Re_c$  [Fig.15(a)] and increasing at high- $Re_c$  [Fig.15(b)] at  $x = -5$ cm. (In Figure 15, the circular symbol is measured data and the solid line inside blind area is an interpolated  $\Delta C_p$  distribution). The upstream pressure increase in front of the SJG is assumed to be due to this stagnation point, but the actual point was not detected at low- $Re_c$ , only becoming more apparent at increasing  $Re_c$  (decreasing both  $C_\mu$  and VR). A small recirculation region is expected to be created by the synthetic jet. Although the static pressure data inside the

blind area is not available, Figure 15 offers some useful indication of the likely flowfield. A low- $Re_c$ , and high- $C_\mu$  (and VR) condition, results in a long recirculation in the region  $-6\text{cm} < x < 19\text{cm}$ , see Figure 15(a). With an increase in  $Re_c$ , the separation point of the CRR is displaced downstream and evidence of a stagnation point begins to appear in the flowfield upstream of the CRR.



(a)  $U=16.18$ ,  $C_\mu=1.67\times 10^{-4}$ ,  $VR=0.68$ ,  $Re_c=1.55\times 10^6$



(b)  $U=24.92$ ,  $C_\mu=7.02\times 10^{-5}$ ,  $VR=0.44$ ,  $Re_c=2.39\times 10^6$

Fig. 15. Interpolated  $\Delta C_p$  distribution in side blind area

### 3.5 Model configuration

In order to suppress the effect of any span-wise flow on the measurements when making measurements in non-zero pressure gradients (not reported here), two simple boundary layer fences are installed on each side of the axial row of pressure tappings, see Figure 16. The boundary layer fences are used when measuring streamwise pressure increment distributions only, all the spanwise pressure measurements were carried out without the boundary layer fences.

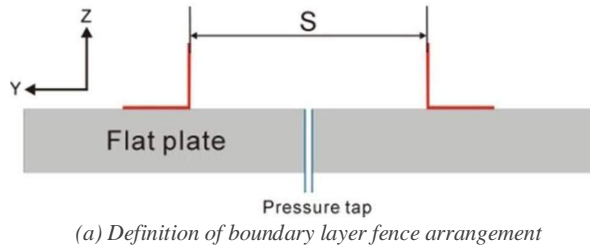


Fig. 16. Boundary layer fence installation on flat plate

### 3.6 Effect of slot yaw angle

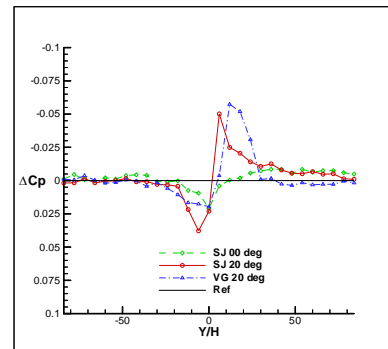
The effect of changes in SJG slot yaw angle ( $\beta$ ) have previously been reported by Kim[10], who shows that  $\beta=20^\circ$  is the optimum. As a result this value is adopted throughout the current study, with data for  $\beta=0^\circ$  being included, where appropriate, for comparison purposes.

### 3.7 Effect of variation in jet momentum coefficient ( $C_{\mu}$ )

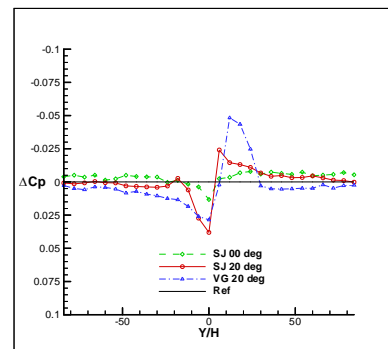
The effect of changes in freestream velocity on the spanwise  $\Delta C_p$  distribution for both the synthetic jet and vane VG in a plane at  $x = 50\text{mm}$  are shown in Figure 17. Given that the SJG excitation frequency is kept constant at the resonance frequency (1.5KHz in this experiment), changes in the freestream flow velocity ( $U$ ) effectively change the jet momentum coefficient ( $C_{\mu}$ ).

As was seen for the measurements made in a zero freestream pressure gradient, regions of +ve and -ve surface static pressure increment are generated downstream around the vortex core. Whilst changes in freestream velocity ( $Re_x$ ) appear to have little influence on the

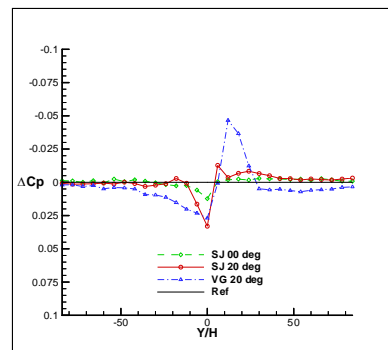
effectiveness of the vane VG, regions of -ve pressure created by the synthetic jet are seen to dissipate with increasing  $Re_x$ . The magnitude of the +ve pressure increment ( $\Delta C_p$ ) caused by the SJG is also reduced with increasing  $Re_x$  but the region influenced does not diminish. This would appear to suggest that, within the limited  $Re_x$  and  $C_{\mu}$  range considered, a synthetic jet has the potential to make small changes to the surface static pressure distribution and could be considered as an effective shape change of an aerofoil at high- $Re_x$  (low- $C_{\mu}$ ), where streamwise vortex is not able to be generated by a synthetic jet.



(a)  $C_{\mu}=5.99 \times 10^{-4}$ ,  $VR=1.30$ ,  $Re_x=1.75 \times 10^5$   $U=8.53\text{m/s}$



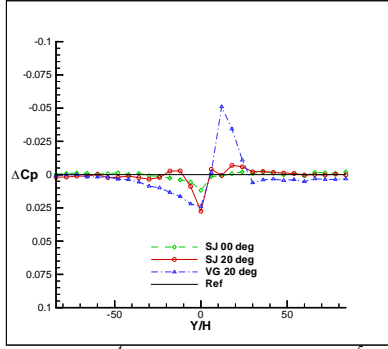
(b)  $C_{\mu}=3.95 \times 10^{-4}$ ,  $VR=1.05$ ,  $Re_x=2.16 \times 10^5$   $U=10.51\text{m/s}$



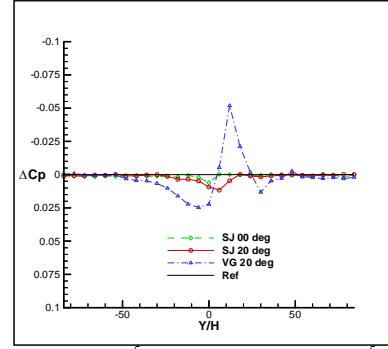
(c)  $C_{\mu}=2.70 \times 10^{-4}$ ,  $VR=0.87$ ,  $Re_x=2.61 \times 10^5$   $U=12.70\text{m/s}$



## THE EFFECT OF A SYNTHETIC JET ON THE PRESSURE DISTRIBUTION OF A FLAT PLATE

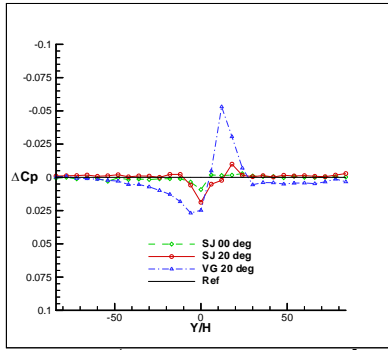


(d)  $C_\mu=2.11 \times 10^{-4}$ ,  $VR=0.77$ ,  $Re_x=2.95 \times 10^5$ ,  $U=14.38\text{m/s}$

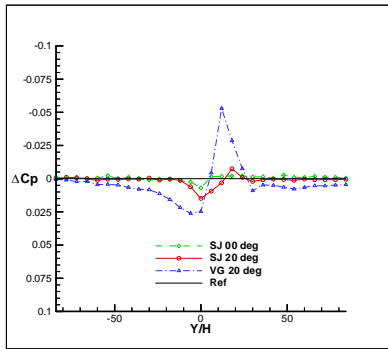


(h)  $C_\mu=6.16 \times 10^{-5}$ ,  $VR=0.42$ ,  $Re_x=5.46 \times 10^5$ ,  $U=26.60\text{m/s}$

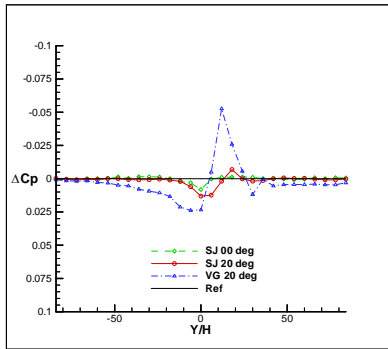
**Fig 17.** Effect of  $C_\mu$  and  $Re_x$  for spanwise  $\Delta C_p$  distribution ( $x=50\text{mm}$ )



(e)  $C_\mu=1.40 \times 10^{-4}$ ,  $VR=0.63$ ,  $Re_x=3.62 \times 10^5$ ,  $U=17.65\text{m/s}$



(f)  $C_\mu=1.12 \times 10^{-4}$ ,  $VR=0.56$ ,  $Re_x=4.05 \times 10^5$ ,  $U=19.76\text{m/s}$



(g)  $C_\mu=1.04 \times 10^{-4}$ ,  $VR=0.54$ ,  $Re_x=4.21 \times 10^5$ ,  $U=20.52\text{m/s}$

### 3.8 Effect of the synthetic jet on the downstream flowfield

Incremental surface static pressure data within the flowfield downstream of both the SJG (slot angle,  $\beta=20^\circ$ ) and the VG, can be used to generate surface pressure contours to aid general comparison of the key flow characteristics, see Figure 18. **The streamwise location of VG is identical with that of SJG ( $x=0\text{mm}$ ).** It is evident that regions of increasing pressure ( $+\Delta C_p$ ), in the flowfield downstream of the vane VG particularly, dominate at the higher Reynolds numbers tested. Whilst the pressure changes which lead to the *virtual aeroshaping* concept have been reported by previous researchers, data which quantifies the lateral extent of the area of increasing pressure has not previously been available.

### 4 Conclusions

Analysis of the surface static pressure distribution on a plate downstream of a both a conventional vane vortex generator and the synthetic jet produced by efflux from an inclined rectangular slot, is used to understand the resulting flow structure. The position of the streamwise vortex core and the sense of the vortex rotation are assessed using the distribution of spanwise pressure coefficient change ( $\Delta C_p$ ). A clear suction peak locates the vortex core and the higher pressure at one side of vortex core represents the downwash of the vortex which implies the sign of vortex rotation.

The magnitude of  $\Delta C_p$  can be used to infer the effect of changes in vortex intensity and vertical displacement.

The effectiveness of a synthetic jet is highly dependent on slot yaw angle ( $\beta$ ). Two SJG angles are investigated  $\beta=0^\circ$  and  $20^\circ$  which exhibit fundamentally different downstream flow features. The SJG with  $\beta=0^\circ$  creates a CVP (Counter-rotating Vortex Pair) within the boundary layer, while  $\beta=20^\circ$  produces a single streamwise vortex. The effect of these two slot yaw angles are compared with a vane type vortex generator ( $\beta=20^\circ$ ). Since  $\beta=20^\circ$  caused higher pressure and suction in the downstream flowfield than  $\beta=0^\circ$ , a single streamwise vortex (caused by  $\beta=20^\circ$ ) is considered to be more effective than a CVP (caused by  $\beta=0^\circ$ ) in terms of its potential for boundary layer control. At a Reynolds number ( $Re_x$ ) of  $1.75 \times 10^5$ , the SJ ( $\beta=20^\circ$ ) produces a greater downstream surface static pressure increments than the conventional vane VG ( $\beta=20^\circ$ ). As for steady jet, the effect of a synthetic jet is seen to diminish with increasing  $Re_x$  (synthetic jet velocity constant) while the effect of a vane VG is seen to be unaffected in the  $Re_x$  range considered.

The streamwise vortices created by a VG ( $\beta=20^\circ$ ) and SJ ( $\beta=20^\circ$ ) drift in a spanwise direction due to the geometric asymmetry of the synthetic jet slot and vortex generator vane. As the vane type vortex generator angle ( $\beta$ ) affects the resulting vortex rotation direction, and the orientation of a synthetic jet slot also affects the resulting streamwise vortex rotation direction. Therefore, by adjusting the slot yaw angle in a multiple slot arrangement, a co-rotating vortex and counter-rotating vortex arrangement can be generated.

A synthetic jet is also seen to affect the flowfield upstream of the slot. At low Reynolds number ( $Re_x=1.17 \times 10^5$ ,  $C_\mu=5.99 \times 10^{-4}$ ), a synthetic jet caused a local pressure reduction at  $x = -50\text{mm}$ , while at high Reynolds number ( $Re_x=3.14 \times 10^5$ ,  $C_\mu=8.29 \times 10^{-5}$ ) a SJG resulted in a pressure increase at the same axial location. This local suction is considered to be due to the

closed recirculation region, which extends to  $x = -50\text{mm}$  at low- $Re_x$ .

mailto:yhkim@emirates.com

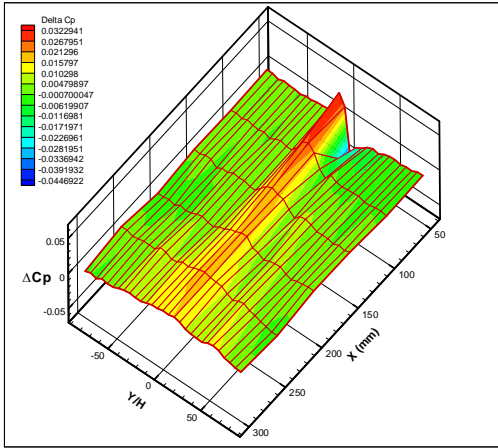
## References

- [1] Young-Hwan KIM, and K.P. Garry. *Time Dependent Analysis of A Rectangular Synthetic Jet*. ICAS 2012, 23 - 28 September 2012, Brisbane, Australia
- [2] K.G. Peterson, R. Funk, and N.M. Komerath, *Recent Experiments on Vortex Collisions with a Cylinder*, AIAA 95-2236, June. 1995
- [3] X.Zhang and M.W.Collins, *Measurements of a longitudinal vortex generated by a rectangular jet in a turbulent boundary layer*, Phys. Fluid Vol. 9, No. 6, 1997
- [4] T.F.Fric and A.Roshko, *Vortical structure in the wake of transverse jet*, J. Fluid Mech, vol 279, pp1-47, 1994
- [5] N.W.Schaeffler and L.N.Jenkins. *The Isolated Synthetic Jet in Crossflow: A Benchmark for Flow Control Simulation*, AIAA 2004-2219, 2004
- [6] C.G.Lomas. *Fundamentals of Hot Wire Anemometry*, Cambridge University Press, 1985
- [7] E.M.Greitzer, C.S.Tan and M.B.Graf *Internal Flow: Concepts and Applications*, Cambridge University Press, 2007.
- [8] J.Proakis and D.G.Manolakis *Digital Signal Processing: Principles, Algorithms, and Applications*, Prentice Hall International Editions
- [9] Murata Manufacturing Company Ltd, "PZT Application Manual".
- [10] Young-Hwan KIM. *The effect of rectangular synthetic jet to the flat plate boundary layer in low Reynolds number*, Experimental Fluid Mechanics 2011, Jičín, Czech Republic, Vol.2, pp 727-746, 2011.
- [11] Young-Hwan KIM *A Parametric Investigation of Synthetic Jet and its Boundary Layer Control*, Ph.D Thesis, Cranfield University, 2005.

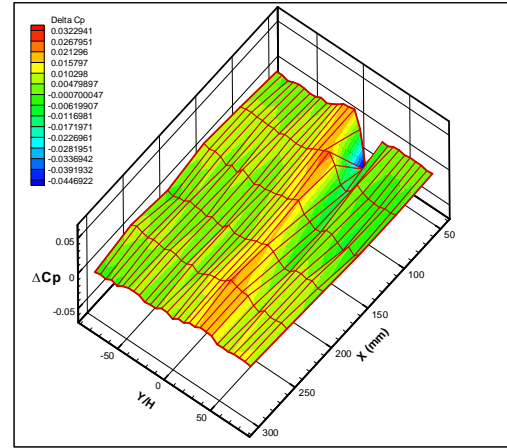
## Copyright Statement

The authors confirm that they, and/or their company or organization, hold copyright on all of the original material included in this paper. The authors also confirm that they have obtained permission, from the copyright holder of any third party material included in this paper, to publish it as part of their paper. The authors confirm that they give permission, or have obtained permission from the copyright holder of this paper, for the publication and distribution of this paper as part of the ICAS 2014 proceedings or as individual off-prints from the proceedings.

**THE EFFECT OF A SYNTHETIC JET ON THE PRESSURE DISTRIBUTION OF A FLAT PLATE**

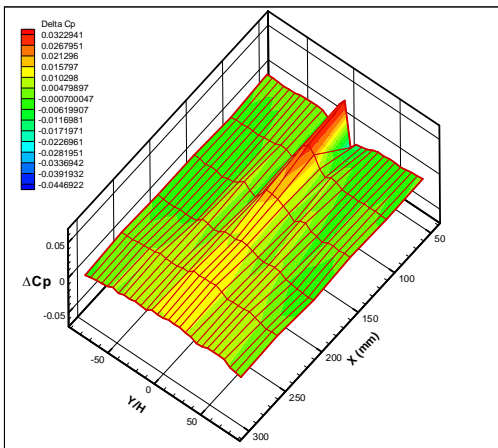


*Synthetic jet*

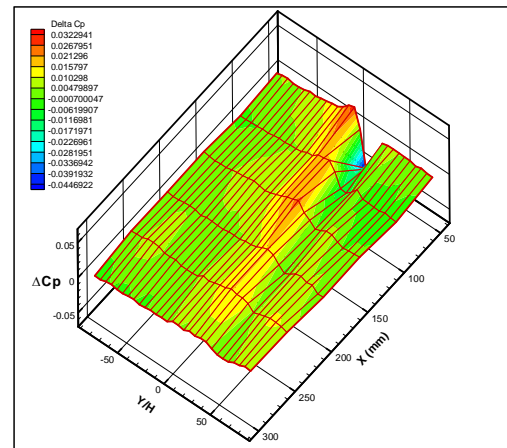


*Vortex generator*

(a)  $U=8.53 \text{ m/s}$ ,  $C_{\mu}=5.99 \times 10^{-4}$ ,  $VR=1.30$ ,  $Re_c=8.17 \times 10^5$

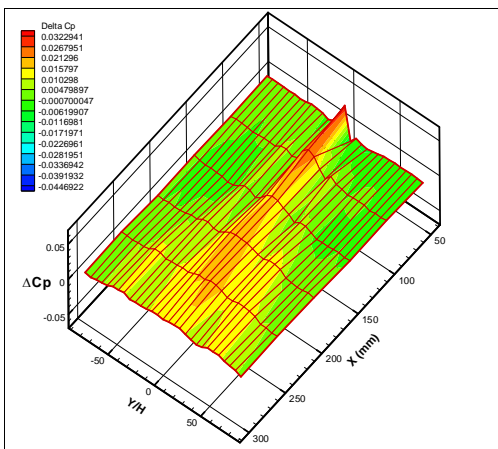


*Synthetic jet*

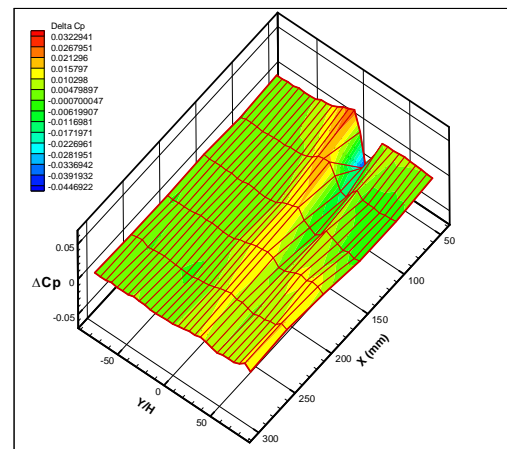


*Vortex generator*

(b)  $U=10.51 \text{ m/s}$ ,  $C_{\mu}=3.95 \times 10^{-4}$ ,  $VR=1.05$ ,  $Re_c=1.01 \times 10^6$

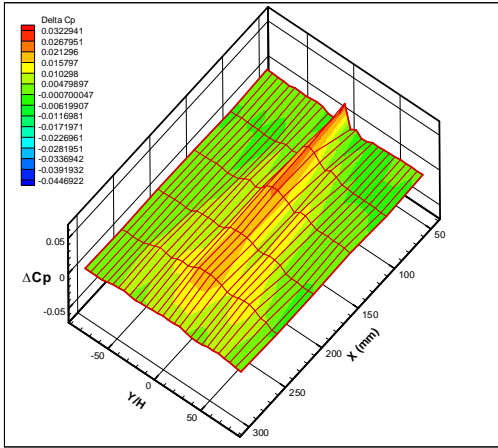


*Synthetic jet*

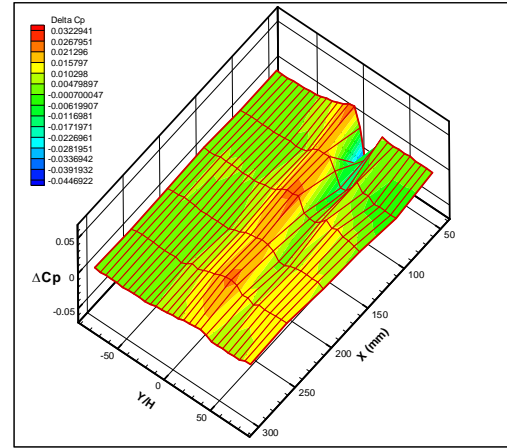


*Vortex generator*

(c)  $U=12.70 \text{ m/s}$ ,  $C_{\mu}=2.70 \times 10^{-4}$ ,  $VR=0.87$ ,  $Re_c=1.22 \times 10^6$

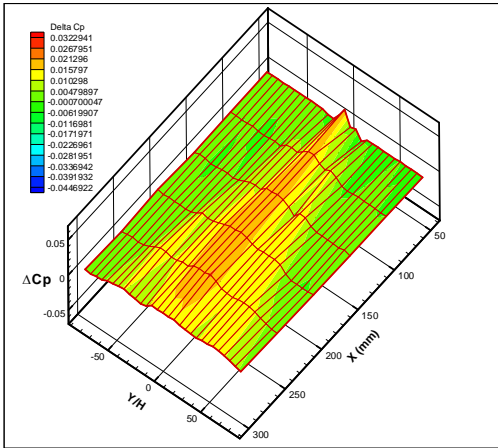


Synthetic jet

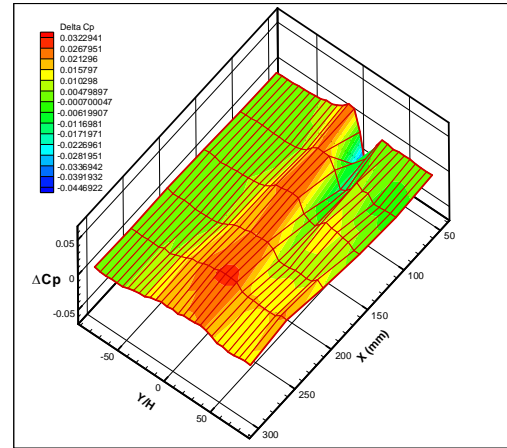


Vortex generator

(d)  $U=14.38\text{m/s}$ ,  $C_{\mu}=2.11 \times 10^{-4}$ ,  $VR=0.77$ ,  $Re_c=1.38 \times 10^6$

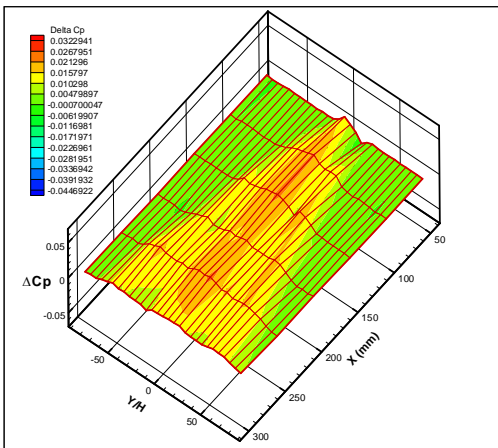


Synthetic jet

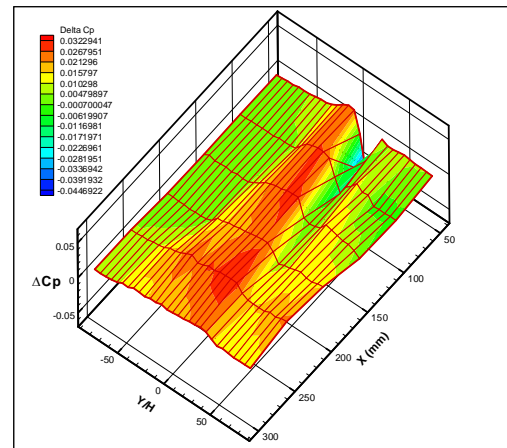


Vortex generator

(e)  $U=16.18\text{m/s}$ ,  $C_{\mu}=1.67 \times 10^{-4}$ ,  $VR=0.68$ ,  $Re_c=1.55 \times 10^6$



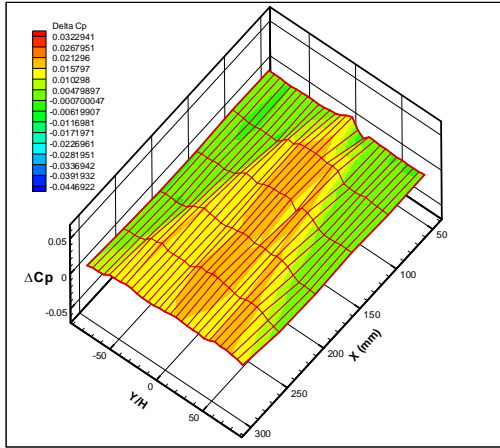
Synthetic jet



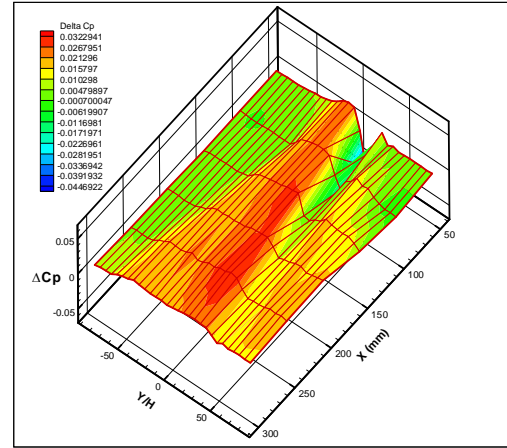
Vortex generator

(f)  $U=19.76\text{m/s}$ ,  $C_{\mu}=1.12 \times 10^{-4}$ ,  $VR=0.56$ ,  $Re_c=1.89 \times 10^6$

**THE EFFECT OF A SYNTHETIC JET ON THE PRESSURE DISTRIBUTION OF A FLAT PLATE**

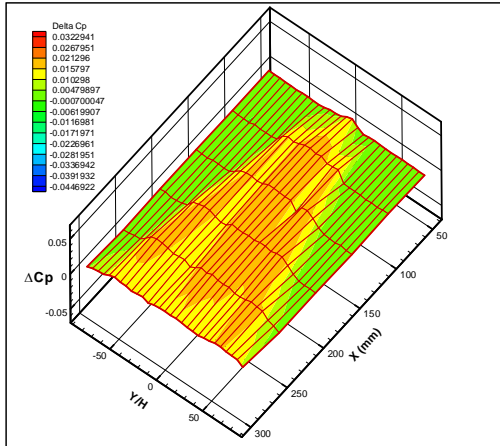


*Synthetic jet*

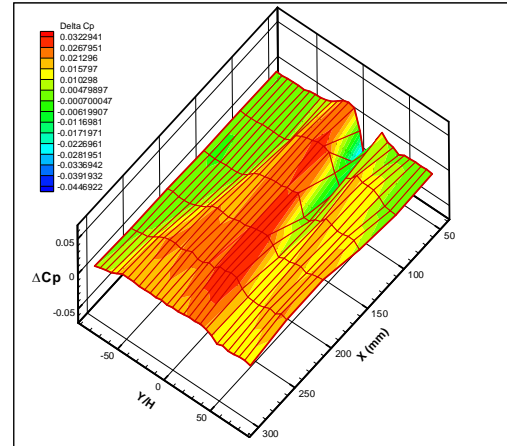


*Vortex generator*

(g)  $U=22.94 \text{ m/s}$ ,  $C_{\mu}=8.28 \times 10^{-5}$ ,  $VR=0.48$ ,  $Re_c=2.20 \times 10^6$



*Synthetic jet*



*Vortex generator*

(h)  $U=26.60 \text{ m/s}$ ,  $C_{\mu}=6.16 \times 10^{-5}$ ,  $VR=0.42$ ,  $Re_c=2.55 \times 10^6$

**Fig. 18.** Static pressure coefficient change ( $\Delta C_p$ ) in the downstream flowfield